IJMMM International Journal of Minerals, Metallurgy and Materials 矿物冶金与材料学报（英文版）

Morphology engineering of ZnO micro/nanostructures under mild conditions for optoelectronic application

Liang Chu, Haoyu Shen, Hudie Wei, Hongyu Chen, Guoqiang Ma, and Wensheng Yan

Cite this article as:
Liang Chu, Haoyu Shen, Hudie Wei, Hongyu Chen, Guoqiang Ma, and Wensheng Yan, Morphology engineering of ZnO micro/nanostructures under mild conditions for optoelectronic application, *Int. J. Miner. Metall. Mater.*, 32(2025), No. 2, pp. 498-503. https://doi.org/10.1007/s12613-024-2965-x

INTERNATIONAL JOURNAL OF
Minerals, Metallurgy and Materials

Volume 32, Number 2, February 2025
Page 498

Research Article https://doi.org/10.1007/s12613-024-2965-x

Morphology engineering of ZnO micro/nanostructures under mild conditions for optoelectronic application

Liang Chu[1),✉], *Haoyu Shen*[1)], *Hudie Wei*[1)], *Hongyu Chen*[1)], *Guoqiang Ma*[2),✉], *and Wensheng Yan*[1),✉]

1) Institute of Carbon Neutrality and New Energy & School of Electronics and Information, Hangzhou Dianzi University, Hangzhou 310018, China
2) School of Applied Physics and Materials, Wuyi University, Jiangmen 529020, China
(Received: 17 March 2024; revised: 29 June 2024; accepted: 1 July 2024)

Abstract: Zinc oxide (ZnO) serves as a crucial functional semiconductor with a wide direct bandgap of approximately 3.37 eV. Solvothermal reaction is commonly used in the synthesis of ZnO micro/nanostructures, given its low cost, simplicity, and easy implementation. Moreover, ZnO morphology engineering has become desirable through the alteration of minor conditions in the reaction process, particularly at room temperature. In this work, ZnO micro/nanostructures were synthesized in a solution by varying the amounts of the ammonia added at low temperatures (including room temperature). The formation of Zn^{2+} complexes by ammonia in the precursor regulated the reaction rate of the morphology engineering of ZnO, which resulted in various structures, such as nanoparticles, nanosheets, microflowers, and single crystals. Finally, the obtained ZnO was used in the optoelectronic application of ultraviolet detectors.

Keywords: morphology engineering; low temperature; ZnO nanosheets; microflowers; ultraviolet detector

1. Introduction

Zinc oxide (ZnO), which is an important semiconductor, possesses excellent physical and chemical properties [1–2]; these properties promote wide applications, such as light-emitting diodes [3–4], ultraviolet (UV) detectors [5–6], gas sensors [7], and solar cells [8–10]. In addition, ZnO is a nontoxic green material, and its synthesis does not introduce toxic materials during the growth process. Importantly, ZnO exhibits direct bandgap of approximately 3.37 eV and low exciton binding energy of 60 meV [11]. Evidently, these unique properties enable ZnO crystals easily absorb UV light and generate electron–hole pairs, which make them suitable for optoelectronic applications, especially UV detectors [5].

ZnO micro/nanostructures vary in terms of physical properties, which results in their improved properties compared with those of bulk ZnO. To date, two primary methods are used for the synthesis of ZnO micro/nanostructures: hydrothermal reaction and chemical vapor deposition [12–15]. The synthesis of ZnO crystals with high-quality and low-density lattice defects can be achieved through chemical vapor deposition; however, such a process requires the use of expensive vacuum equipment [16]. The solution in the hydrothermal reaction of ZnO is usually aqueous, and the growth mechanism shows a close relation to external conditions, such as solution pH [17], temperature, reaction concentration, and additive [12]. This method is conventionally used for the synthesis of various ZnO micro/nanostructures. However, this synthesis procedure often requires the use of an autoclave, which implies high energy consumption and load-bearing requirements. ZnO morphology engineering can also influence the performance of specific applications. Therefore, the synthesis of ZnO micro/nanostructures with morphology engineering under mild conditions, including at room temperature, remains a challenge.

In this work, a facile solution method was developed to prepare ZnO micro/nanostructures at room temperature using precursors containing zinc nitrate ($Zn(NO_3)_2·6H_2O$), sodium hydroxide (NaOH), and ammonia ($NH_3·H_2O$) solution. In particular, the concentration of $NH_3·H_2O$ plays a crucial role in controlling the reaction rate for morphology engineering [18–19]. Adjustment of the morphology of ZnO micro/nanostructures, from random nanoparticles to regular nanosheets, microflowers, and single crystals, can be achieved. This approach paves a novel means to fabricate ZnO micro/nanostructures under low-cost, mild, and environment-friendly conditions. ZnO microflowers and nanosheets were used in interdigitated-electrode UV detectors. The microflower-based device exhibited high performance and operation stability based on the band structure and three-dimensional light capture.

2. Experimental

The raw materials included $Zn(NO_3)_2·6H_2O$, NaOH, and $NH_3·H_2O$ solution (25%–28%). $Zn(NO_3)_2·6H_2O$ and NaOH

✉ Corresponding authors: Liang Chu E-mail: chuliang@hdu.edu.cn; Guoqiang Ma E-mail: mgq1103@163.com;
Wensheng Yan E-mail: wensheng.yan@hdu.edu.cn

Springer

served as sources of Zn^{2+} and OH^-, respectively. $NH_3{\cdot}H_2O$ can be combined with Zn^{2+} to tune the reaction rate on the effect of ZnO product structures. As shown in Fig. 1, 1.16 g $Zn(NO_3)_2{\cdot}6H_2O$ was dissolved in 130 mL distilled water with stirring typically, and then $NH_3{\cdot}H_2O$ solution (1–6 mL) was slowly added to the solution and mixed well to achieve full complexation. During this period, the solution immediately turned turbid and clarified. Next, 0.288 g NaOH was dissolved in 6 mL distilled water completely by ultrasound, which was slowly added dropwise to the above solution under stirring. Finally, the chemical reaction was kept at room temperature 50, 70, and 90°C, respectively. After the reaction, the white precipitates were washed with deionized water and dried at 70°C in an oven overnight.

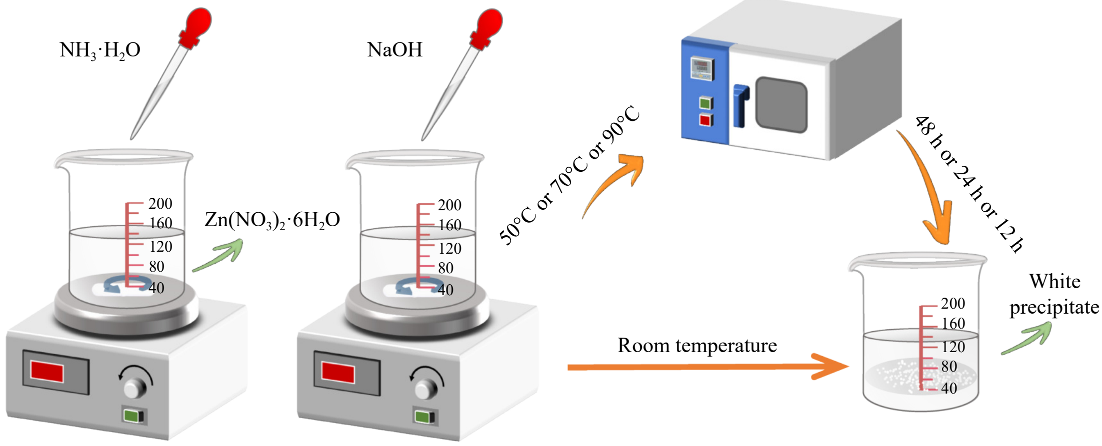

Fig. 1. Schematic diagram of the synthesis process for ZnO micro/nanostructures.

Flexible polyethylene terephthalate (PET) substrates were washed with deionized water and ethanol and dried via N_2 flow. Then, the Au electrodes were deposited on the flexible PET substrates through thermal evaporation, and the interdigitated 20 fingers (width 100 µm, interfinger spacing 100 µm, and length 10 mm) were patterned by UV lithography. The ZnO powders exhibited dispersion in ethanol, deposition on the interdigitated Au electrodes, and drying at 70°C to form flexible UV detectors.

The phase of the obtained white powders was checked via X-ray diffraction (XRD) pattern with Cu-K$_\alpha$ irradiation (λ = 1.5418 Å, Bruker D8 Advance X-ray diffractometer). The morphology was characterized via scanning electron microscopy (SEM, FEI NOVA Nano SEM 450) and transmission electron microscopy (TEM, JEOL/JEM-F200). The UV–visible light absorption was measured using a LAMBDA 1050 spectrometer (PerkinElmer). Regarding the UV detector, the current–voltage (I–V) and current–time (I–t) curves were measured on electrochemical workstation (Model 600E Series). The UV light was originated from a light source (365 nm, ZF-1, Shanghai ChiTang Industrial Co. Ltd).

3. Results and discussion

3.1. Structural and morphological characterization

Fig. 2 shows the XRD patterns of the obtained white precipitates. The diffraction peaks at 31.5°, 34.1°, 36.0°, 47.2°, 56.3°, 62.6°, 67.6°, 68.8°, and 77.0° can be indexed to the (100), (002), (101), (102), (110), (103), (112), (201), and (202) planes of hexagonal wurtzite ZnO phase (JCPDS No. 36-1451), respectively [18–19]. Evidently, when the NaOH solution was directly added to the $Zn(NO_3)_2{\cdot}6H_2O$ solution, the white ZnO precipitates formed immediately. In the product XRD pattern, an additional peak was located at 25.83°. If the $NH_3{\cdot}H_2O$ solution participated in the reaction, the resulting products also comprised the ZnO phase. The more $NH_3{\cdot}H_2O$ added, the lower the recreation rate. Thus, low chemical reaction rate can improve the crystallinity, and thus, with the increase in $NH_3{\cdot}H_2O$ amount, the diffraction peak intensities of ZnO products showed a gradual increase.

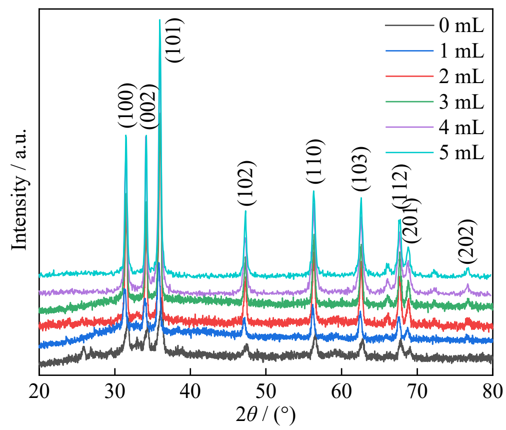

Fig. 2. XRD patterns of ZnO micro/nanostructures synthesized using various amounts of $NH_3{\cdot}H_2O$ solution.

The chemical reaction can be expressed as follows [18–19]:

$$Zn^{2+} + NH_3 \leftrightarrow Zn(NH_3)_x^{2+}\ (x = 1, 2, 3, 4) \quad (1)$$

$$Zn^{2+} + 4OH^- \rightarrow Zn(OH)_4^{2-} \quad (2)$$

$$Zn(OH)_4^{2-} \rightarrow ZnO + H_2O + 2OH^- \quad (3)$$

The synthesis of ZnO precipitates can be divided into three stages. First, Zn^{2+} ions were combined with NH_3 from the $NH_3{\cdot}H_2O$ solution to form ion complexes of $Zn(NH_3)_x^{2+}$

(x = 1, 2, 3, 4). When the $NH_3·H_2O$ solution was added to the $Zn(NO_3)_2$ solution, the solution immediately turned turbid and clarified under rocking. The $Zn(NH_3)_x^{2+}$ complexes slowly released Zn^{2+} after the addition of OH^- to form $Zn(OH)_4^{2-}$ [20]. Finally, the $Zn(OH)_4^{2-}$ was transferred to the stable ZnO phase. Therefore, the amount of $NH_3·H_2O$ added can be used to manage the reaction rate of the synthesized ZnO [21]. The increase in $NH_3·H_2O$ amount led to high degree of complexation, which slowed down the reaction rate of ZnO. In contrast, heating speeds up this release process. Thus, the higher the temperature, the faster the reaction rate.

Room-temperature chemical reactions (about 20°C) offer evident advantages. Typically, the process saves energy and facilitates product generation without requiring high-temperature condition. This provides an idea for mass production in industrialization. In this work, room-temperature reaction was first carried out. The dose of the added $NH_3·H_2O$ solution was increased from 0 to 6 mL, with a step of 1 mL. The samples synthesized under the $NH_3·H_2O$ doses from 0 to 4 mL comprised white precipitates. If the $NH_3·H_2O$ solution increased to 5 mL, the products cannot be obtained immediately, and the reaction consumed a considerable amount of time. After 5 d, millimeter-sized crystals can be evidently observed. In particular, when 6 mL or more $NH_3·H_2O$ was added, no product can be observed at room temperature. Heating can increase the reaction activity [22–23]. The increase in the temperature may enable the synthesis of ZnO with $NH_3·H_2O$ addition of 6 mL or more. Dried white precipitates were obtained after the reaction under heat.

SEM and TEM were applied in the investigation of the morphology of ZnO products. Fig. 3 shows the morphology of the ZnO synthesized at room temperature using various amounts of $NH_3·H_2O$. In the absence of $NH_3·H_2O$, the reaction occurred quickly, which led to the random and aggregated morphology of ZnO nanoparticles (Fig. 3(a)). After the addition of 1 mL $NH_3·H_2O$ in the reaction, the products also aggregated but assumed sheet shape with microscale surface (Fig. 3(b)). Evident ZnO nanosheets were observed when 2 mL $NH_3·H_2O$ was used (Fig. 3(c)). With the increase in $NH_3·H_2O$ to 3 mL (Fig. 3(d)), the nanosheets become more evident and regular with sizes of 3–5 µm. Moreover, the sheets gradually became thinner. On the one hand, the increase in $NH_3·H_2O$ concentration reduced the reaction rate. On the other hand, stirring the reaction solution provided tangential shear force. Therefore, two-dimensional (2D) ZnO nanosheets can be formed at an appropriate $NH_3·H_2O$ concentration. When the $NH_3·H_2O$ added was increased to 4 mL, the nanosheets thickened due to the slow reaction rate (Fig. 3(e)), and the size of the nanosheets decreased to approximately 1 µm. When the $NH_3·H_2O$ concentration was increased to 5 mL, the reaction rate further slowed down, and the product transformed into macroscopic and millimeter-scale single crystals after 5 d (Fig. 3(f)).

The 2D ZnO nanosheets were also characterized via TEM technology. Fig. 4(a) shows a typical 2D ZnO nanosheet having the polycrystalline characteristics observed from the selected area electron diffraction (SAED) (Fig. 4(b)). The spotted rings corresponded to the (100), (002), (101), (102), (110), and (103) lattice planes of hexagonal wurtzite ZnO. The high-resolution TEM image in Fig. 4(c) reveals that the lattice fringes with distances of 0.284 (0.287) and 0.267 nm (0.268 nm) were indexed to the ZnO (100) and (002) planes, respectively. The random domains further conformed to the polycrystalline nature of 2D ZnO nanosheets. To the best of our knowledge, this phenomenon is the first documentation of polycrystalline 2D ZnO nanosheets [24].

Given the presence of the reaction with 6 mL $NH_3·H_2O$ addition at room temperature, the temperature was set to 50, 70, and 90°C. The required reaction times periods varied with temperature. The reaction times under 50, 70, and 90°C las-

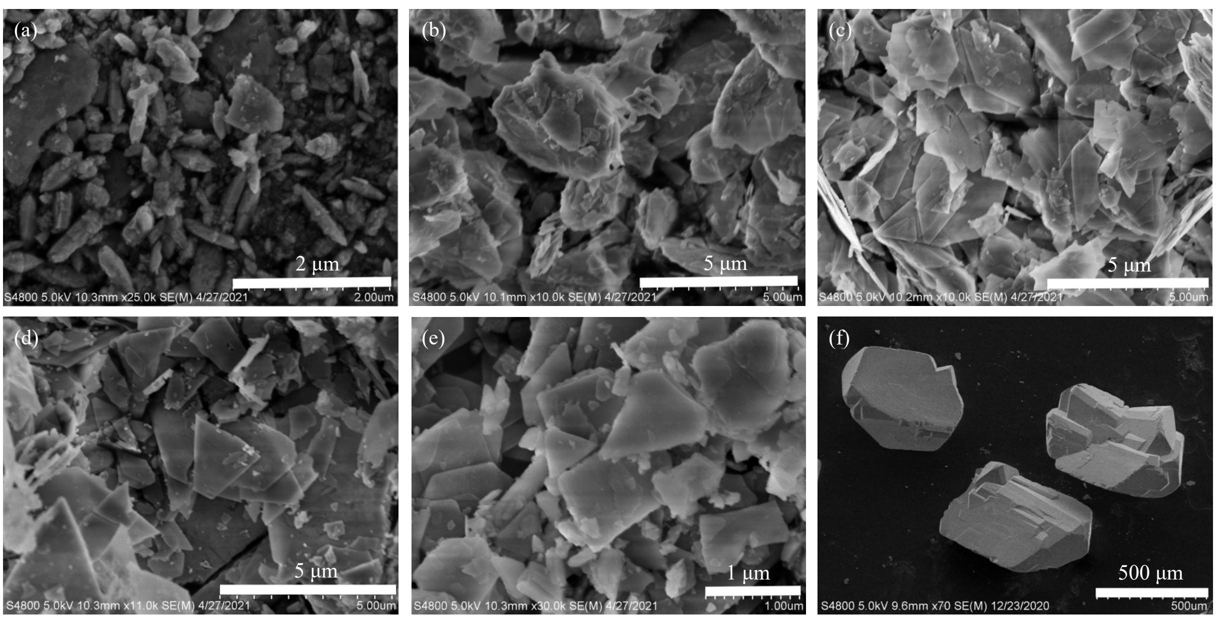

Fig. 3. SEM images of ZnO micro/nanostructures synthesized at room temperature using various amount of $NH_3·H_2O$: (a) 0; (b) 1 mL; (c) 2 mL; (d) 3 mL; (e) 4 mL; (f) 5 mL.

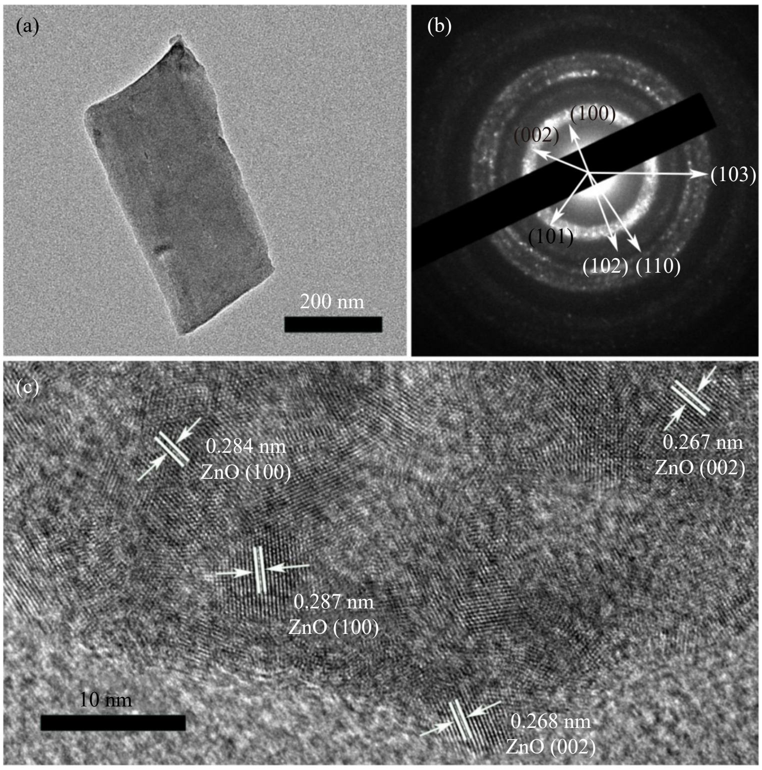

Fig. 4. (a) TEM image, (b) selected area electron diffraction, and (c) high-resolution TEM image of the typical ZnO nanosheet.

ted for 48, 24, and 12 h, respectively, with the corresponding SEM images displayed in Fig. 5(a)–(c). All products had microflower morphology, which was composed of nanorods. As the temperature rose to 90°C, some microflowers collapsed as independent nanorods due to the rapid reaction rate. Consequently, moderate temperature aids in attaining more regular morphology.

The reaction rate slowed down with the increased amount of $NH_3 \cdot H_2O$ addition. Moreover, when the $NH_3 \cdot H_2O$ reached 4 mL, the ZnO nanosheets thickened due to the slower reaction rate, and the output of immediately collected ZnO precipitates decreased at room temperature. Thus, when the temperature was set at 70°C, the $NH_3 \cdot H_2O$ amount begin from 4 mL. Fig. 5(d)–(f) shows the SEM images of the ZnO synthesized at 70°C with $NH_3 \cdot H_2O$ addition of 4, 5, and 7 mL, respectively. Fig. 5(d) shows the presence of microflowers and microspheres comprising nanoparticles and nanorods. Regular ZnO microflowers were obtained when the $NH_3 \cdot H_2O$ addition increased to 5 and 6 mL, as shown in Fig. 5(e) and Fig. 5(b), respectively. When it further increased to 7 mL, excessive $NH_3 \cdot H_2O$ led to high-alkaline environment, which destroyed the ZnO products to random aggregation of

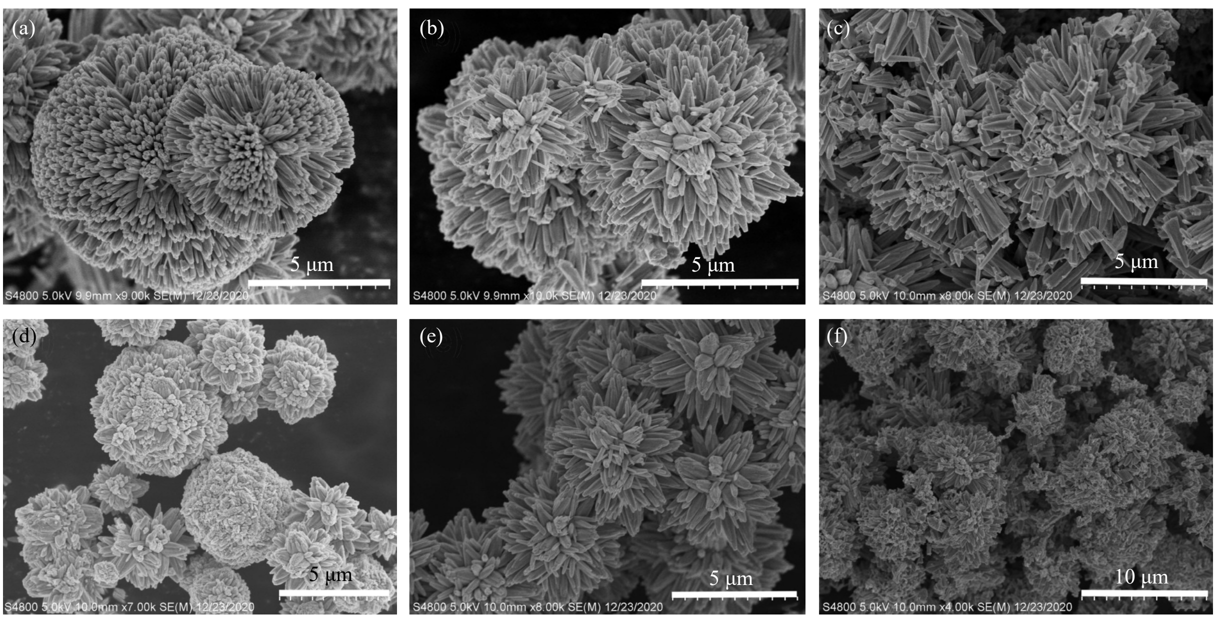

Fig. 5. SEM images of ZnO structures synthesized at various temperatures and $NH_3 \cdot H_2O$: (a) 50°C, 6 mL; (b) 70°C, 6 mL; (c) 90°C, 6 mL; (d) 70°C, 4 mL; (e) 70°C, 5 mL; (f) 70°C, 7 mL.

nanoparticles (Fig. 5(f)).

3.2. Optoelectronic application

The ZnO microflowers synthesized using 5 mL $NH_3 \cdot H_2O$ addition at 70°C can accomplish 3D light capture, which enables the efficient absorption of UV light (Fig. S1, see the supplementary material) [25]. The ZnO microflowers were further applied to the UV detector (Fig. 6). Fig. 6(a) shows the *I*–*V* curves of the UV detectors in the dark and under 365 nm UV, and Fig. 6(b) displays the amplified dark current. An evident photocurrent of the ZnO UV detectors was observed. The calculated light on/off ratio at 1 V was approximately 50. In addition, the Schottky contacts formed between ZnO microflowers and Au electrodes. Fig. 6(c) shows the switching curve of current in the dark and under UV illumination with a constant bias voltage of 1.0 V. The rising and decaying photocurrents obey the exponential function, which can be fitted with the corresponding time. The two exponential function Eqs. (4) and (5) used for respective rising and decaying photocurrents (I_t) with the time (t) are expressed as follows [26–27]: The two exponential function Eqs. (4) and (5) used for respective rising and decaying photocurrents (I_t) with the time (t) are expressed as follows

$$I_t = I_0 + A_1\left(1 - e^{-\frac{t}{\tau_{r1}}}\right) \tag{4}$$

$$I_t = I_0 + A_2 e^{-\frac{t}{\tau_{d1}}} + A_3 e^{-\frac{t}{\tau_{d2}}} \tag{5}$$

where I_0 denotes the dark current, A_1, A_2, and A_3 indicate positive constants, τ_{r1} and τ_d (τ_{d1} and τ_{d2}) are time constants for rising and decaying photocurrents, respectively. On the basis of curve fittings, the rise time constant for ZnO was τ_{r1} = 21.3 s, and the decay time constants were τ_{d1} = 13.7 s and τ_{d2} = 36.3 s, which are similar to the previous results on ZnO nanowire arrays [26–27]. In addition, the UV sensitivity of 2D ZnO nanosheets was measured (Fig. S2). The photocurrent is lower than that of the microflower-based device. Therefore, the obtained ZnO microflowers can be applied as excellent UV detectors.

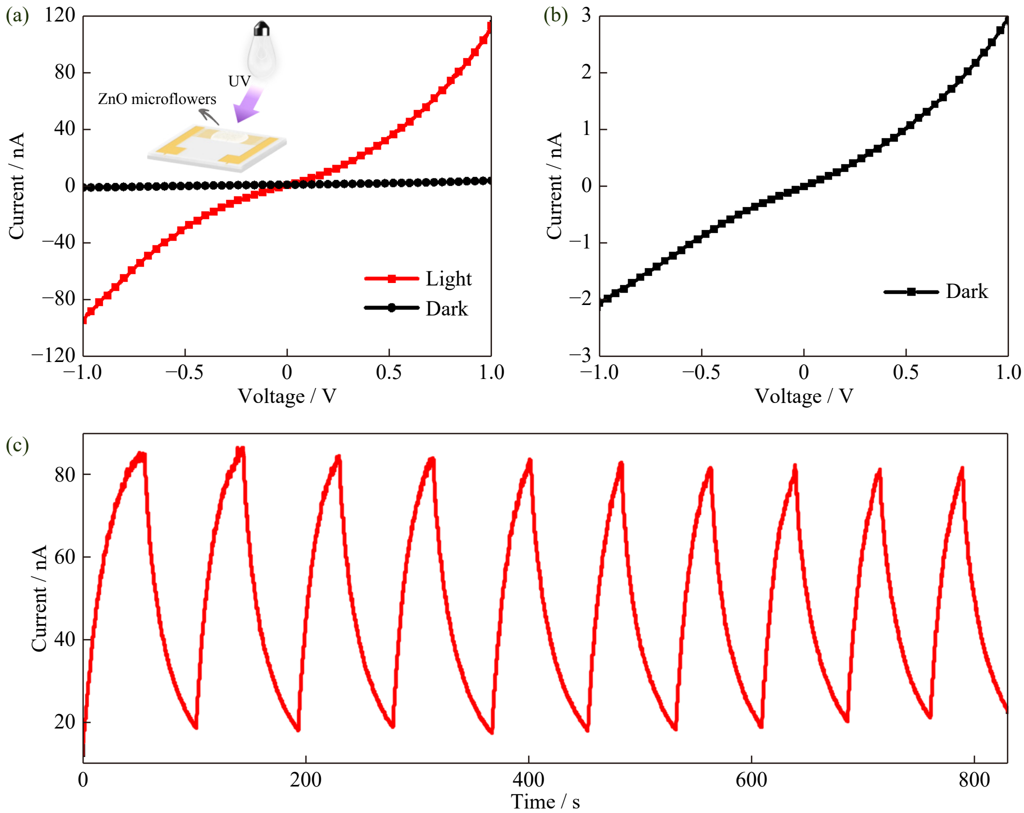

Fig. 6. (a) *I*–*V* characteristics of ZnO-microflower-based UV detectors with and without 365 nm UV illumination, (b) *I*–*V* characteristics of ZnO UV detectors without light irradiance and (c) reversible switching of electrical current for ZnO detector at 1 V biasing voltage in the dark state and under 365 nm UV illumination.

4. Conclusion

ZnO micro/nanostructures were prepared through simple and low-cost hydrothermal method, nearly at room temperature, through the introduction of $NH_3 \cdot H_2O$ solution. The NH_3 in $NH_3 \cdot H_2O$ solution combined with the Zn^{2+} precursor to form complexes, which can be used to tune the reaction rate and influence of the resulting ZnO structures. At a precise amount of $NH_3 \cdot H_2O$ addition, the polycrystalline 2D ZnO nanosheets can be obtained as a result of the stirring-induced tangential shear force at room temperature. Meanwhile, during relatively slow reaction, ZnO single crystals formed after 5 d at room temperature. Heating (such as 70°C) can increase the reaction rate, which leads to 3D microflowers. The ZnO microflowers can effectively capture UV light as detectors. Therefore, this facile and low-cost synthesis method can be applied in tuning ZnO micro/nanostructures and be easily scaled-up for industrial production, which will promote their optoelectronic applications, typically in UV detectors.

Acknowledgements

This work was funded by the National Natural Science Foundation of China (No. 52172205).

Conflict of Interest

The authors declare that they have no financial or proprietary interests that influence the reporting of this article.

Supplementary Information

The online version contains supplementary material available at https://doi.org/10.1007/s12613-024-2965-x.

References

[1] Y.D. Gu, W.J. Mai, and P. Jiang, Characterization of structural and electrical properties of ZnO tetrapods, *Int. J. Miner. Metall. Mater.*, 18(2011), No. 6, p. 686.

[2] S. Suwanboon, P. Amornpitoksuk, P. Bangrak, and C. Randorn, Physical and chemical properties of multifunctional ZnO nanostructures prepared by precipitation and hydrothermal methods, *Ceram. Int.*, 40(2014), No. 1, p. 975.

[3] E. Moyen, J.H. Kim, J. Kim, and J. Jang, ZnO nanoparticles for quantum-dot-based light-emitting diodes, *ACS Appl. Nano Mater.*, 3(2020), No. 6, p. 5203.

[4] G.C. Park, S.M. Hwang, S.M. Lee, *et al.*, Hydrothermally grown in-doped ZnO nanorods on p-GaN films for color-tunable heterojunction light-emitting-diodes, *Sci. Rep.*, 5(2015), art. No. 10410.

[5] Y. Li, F. Della Valle, M. Simonnet, I. Yamada, and J.J. Delaunay, High-performance UV detector made of ultra-long ZnO bridging nanowires, *Nanotechnology*, 20(2009), No. 4, art. No. 045501.

[6] Y. Ning, Z.M. Zhang, F. Teng, and X.S. Fang, Novel transparent and self-powered UV photodetector based on crossed ZnO nanofiber array homojunction, *Small*, 14(2018), No. 13, art. No. 1703754.

[7] S.K. Gupta, A. Joshi, and M. Kaur, Development of gas sensors using ZnO nanostructures, *J. Chem. Sci.*, 122(2010), No. 1, p. 57.

[8] S.J. Li, Y. Lin, W.W. Tan, *et al.*, Preparation and performance of dye-sensitized solar cells based on ZnO-modified TiO_2 electrodes, *Int. J. Miner. Metall. Mater.*, 17(2010), No. 1, p. 92.

[9] V. Consonni, J. Briscoe, E. Kärber, X. Li, and T. Cossuet, ZnO nanowires for solar cells: A comprehensive review, *Nanotechnology*, 30(2019), No. 36, art. No. 362001.

[10] P. Fan, D.Y. Zhang, Y. Wu, J.S. Yu, and T.P. Russell, Polymer-modified ZnO nanoparticles as electron transport layer for polymer-based solar cells, *Adv. Funct. Mater.*, 30(2020), No. 32, art. No. 2002932.

[11] K. Lim, W.S. Chow, and S.Y. Pung, Enhancement of thermal stability and UV resistance of halloysite nanotubes using zinc oxide functionalization *via* a solvent-free approach, *Int. J. Miner. Metall. Mater.*, 26(2019), No. 6, p. 787.

[12] H.M. Shao, X.Y. Shen, X.T. Li, *et al.*, Growth mechanism and photocatalytic evaluation of flower-like ZnO micro-structures prepared with SDBS assistance, *Int. J. Miner. Metall. Mater.*, 28(2021), No. 4, p. 729.

[13] V. Gerbreders, M. Krasovska, E. Sledevskis, *et al.*, Hydrothermal synthesis of ZnO nanostructures with controllable morphology change, *CrystEngComm*, 22(2020), No. 8, p. 1346.

[14] L.V. Podrezova, S. Porro, V. Cauda, M. Fontana, and G. Cicero, Comparison between ZnO nanowires grown by chemical vapor deposition and hydrothermal synthesis, *Appl. Phys. A*, 113(2013), No. 3, p. 623.

[15] Y.P. Zhao, C.C. Li, M.M. Chen, *et al.*, Growth of aligned ZnO nanowires via modified atmospheric pressure chemical vapor deposition, *Phys. Lett. A*, 380(2016), No. 47, p. 3993.

[16] Y.B. He, L.H. Wang, L. Zhang, *et al.*, Solubility limits and phase structures in epitaxial ZnOS alloy films grown by pulsed laser deposition, *J. Alloys Compd.*, 534(2012), p. 81.

[17] Y. Zhou, D. Li, X.C. Zhang, J.L. Chen, and S.Y. Zhang, Facile synthesis of ZnO micro-nanostructures with controllable morphology and their applications in dye-sensitized solar cells, *Appl. Surf. Sci.*, 261(2012), p. 759.

[18] C.K. Xu, P. Shin, L.L. Cao, and D. Gao, Preferential growth of long ZnO nanowire array and its application in dye-sensitized solar cells, *J. Phys. Chem. C*, 114(2010), No. 1, p. 125.

[19] Y.F. Gao, M. Nagai, T.C. Chang, and J.J. Shyue, Solution-derived ZnO nanowire array film as photoelectrode in dye-sensitized solar cells, *Cryst. Growth Des.*, 7(2007), No. 12, p. 2467.

[20] J.M. Wang and L. Gao, Synthesis and characterization of ZnO nanoparticles assembled in one-dimensional order, *Inorg. Chem. Commun.*, 6(2003), No. 7, p. 877.

[21] Y.F. Chen, X.J. Yang, and S.H. Zhou, Structure and photoluminescence of ZnO/niobate composites self-assembled from Zn $(NH_3)_4^{2+}$ solution with different pH and contents, *J. Non-Cryst. Solids*, 356(2010), No. 9-10, p. 509.

[22] G. Sathishkumar, C. Rajkuberan, K. Manikandan, S. Prabukumar, J. DanielJohn, and S. Sivaramakrishnan, Facile biosynthesis of antimicrobial zinc oxide (ZnO) nanoflakes using leaf extract of *Couroupita guianensis Aubl.*, *Mater. Lett.*, 188(2017), p. 383.

[23] H. Savaloni and R. Savari, Nano-structural variations of ZnO: N thin films as a function of deposition angle and annealing conditions: XRD, AFM, FESEM and EDS analyses, *Mater. Chem. Phys.*, 214(2018), p. 402.

[24] J. Safaei and G.X. Wang, Progress and prospects of two-dimensional materials for membrane-based osmotic power generation, *Nano Res. Energy*, 1(2022), art. No. e9120008.

[25] Z. Chen, J.F. Li, T.Z. Li, *et al.*, A CRISPR/Cas12a-empowered surface plasmon resonance platform for rapid and specific diagnosis of the Omicron variant of SARS–CoV–2, *Natl. Sci. Rev.*, 9(2022), No. 8, art. No. nwac104.

[26] X.H. Zhang, X.Y. Han, J. Su, Q. Zhang, and Y.H. Gao, Well vertically aligned ZnO nanowire arrays with an ultra-fast recovery time for UV photodetector, *Appl. Phys. A*, 107(2012), No. 2, p. 255.

[27] D. Gedamu, I. Paulowicz, S. Kaps, *et al.*, Rapid fabrication technique for interpenetrated ZnO nanotetrapod networks for fast UV sensors, *Adv. Mater.*, 26(2014), No. 10, p. 1541.